Applied Catalysis B: Environmental 321 (2023) 122042

Contents lists available at ScienceDirect

Applied Catalysis B: Environmental

journal homepage: www.elsevier.com/locate/apcatb

A green, efficient reductive N-formylation of nitro compounds catalyzed by metal-free graphitic carbon nitride supported on activated carbon

Xing Wang, Xiaona Liu, Hui Wen, Kai Guo, Hlomayi Brendon, Di Liu *

College of Chemical and Biological Engineering, Shandong University of Science and Technology, Qingdao 266590, PR China

ARTICLE INFO

Keywords:
Formylation
Metal-free catalysis
Carbon nitride
Activated carbon
Carbon defect

ABSTRACT

Metal-free graphitic carbon nitride supported on activated carbon was fabricated via a simple pyrolysis for one-pot reductive N-formylation of nitro compounds with formic acid and sodium formate was employed as promoter. Under the conditions, this transformation was successfully achieved without any solvent. The support activated carbon and pyrolysis atmosphere had important influence on catalytic behavior of catalyst. SEM, TEM, XRD, XPS, EPR, FT-IR, Raman spectrum and N_2 adsorption/desorption characterizations revealed that air pyrolysis enabled g-C_3N_4 to generate more carbon defects and the support AC effectively dispersed g-C_3N_4 to expose more active sites. Using our procedure, a broad set of nitro compounds was converted to their corresponding formamides with various functional group tolerances. The catalyst could be recycled several times without marked loss of activity. In short, we provided an efficient and sustainable protocol for the expedient synthesis of formamides from nitro compounds.

1. Introduction

The amide bond is pervasive in nature and one of the most important functional groups. A comprehensive survey exhibited that more than 25% of known drugs contained an amide group [1]. Among various amides, formamides have been extensively applied in pharmaceuticals, fragrances, agrochemicals, dyes and polymers [2,3]. Moreover, formamides serve as industrial solvents [4] and catalyst [5]. Thus, the production of formamide has attracted considerable attention. In the past decades, it was extensively studied to synthesize N-formamides by the condensation of amines with formylating reagents, such as methanol [6,7], formic acid [8–12] and (para)-formaldehyde [13]. However, this route suffers from the drawbacks of the production of massive wastes and unsatisfactory atom-efficiency. Therefore, it is desirable to develop an economical, environmentally friendly and greener process in organic chemistry and industry.

Recently, a novel protocol, the one-pot direct reductive N-formylations of nitro compounds to N-formamides, was developed [14]. The successive multistep transformation involves hydrogen production, transfer hydrogenation of nitro compounds and the condensation of amines with formylating reagents. Compared with N-formylations of amines to N-formamides, this synthetic route avoids hydrogenation process of nitro compounds as well as associated separation and purification steps. Obviously, formylating reagents have played a key role in the transformation. Formic acid (FA), as a renewable material, is an easy-to-handle liquid hydrogen donor with 4.4 wt% hydrogen content, and it can also be used as the formylating reagents. So, FA is an excellent alternative as hydrogen and formylating source for this transformation. To date, the direct reductive N-formylations of nitro compounds with formic acid to N-formamides were usually achieved in the presence of metal catalysts including noble metal (e.g. Pd [15,16], Au [17], Rh [18], etc.) and non-noble metal (Co[19,20] and Zn[21,22]). These metal catalytic systems exhibit considerable advances, whereas there are different levels of drawbacks. Firstly, the reagent FA generates acidic environment, so the leaching of metal is almost inevitable for these metal catalysts, resulting in the decline of catalytic performance of catalyst as well as metal pollution of product. Moreover, the scarcity and high cost of metal catalysts (especially noble metal catalysts) impede their practical applications. Therefore, there exists growing incentive to develop an inexpensive and efficient catalyst for the reductive N-formylations of nitro compounds to formamides. If we can design a kind of metal-free catalyst for the reductive N-formylations of nitro compounds with FA, it would avoid the use of noble metal and the leaching of metal catalyst fundamentally. Based on the aim, this study is committed to exploring a metal-free catalyst and eco-friendly protocol for the reductive N-formylations of nitro compounds with FA to formamides. To the

* Correspondence to: 579 Qianwangang Road, Economic & Technical Development Zone, Qingdao, Shandong 266590, PR China.
E-mail address: ld002037132@163.com (D. Liu).

https://doi.org/10.1016/j.apcatb.2022.122042
Received 22 July 2022; Received in revised form 16 September 2022; Accepted 3 October 2022
Available online 4 October 2022
0926-3373/© 2022 Elsevier B.V. All rights reserved.

best of our knowledge, there are no reports of non-metallic catalysts for this transformation.

Carbon materials, such as carbon nanotubes [23,24], graphene [25], carbon nitride [26], have attracted extensive interests in many fields. Among these, carbon nitride is widely studied in the catalysis field due to unique structure, electronic properties, low cost and non-pollution. For instance, g-C_3N_4 has been applied in photocatalysis [27,28], environmental protection [29–31] and electrochemistry [32]. And beyond that, g-C_3N_4 was also used as heterogeneous catalyst in organic reaction (e.g Friedel-Crafts reaction [33], Knoevenagel condensation [34] and acetylene hydrochlorination [35]).

Herein, we developed an effective g-C_3N_4 supported on activated carbon (AC) as metal-free catalyst for the one-pot reductive N-formylations of nitro compounds to formamides. And, formic acid-sodium formate (SF) system was employed innovatively as hydrogen source to improve the reaction efficiency. The relationship between catalyst property and catalytic performance of g-C_3N_4 supported on activated carbon was discussed and a green and efficient protocol of N-formylations of nitro compounds to formamides was established.

2. Experimental section

2.1. Materials

Activated carbon was obtained from Xilong Scientific Co., Ltd. Other chemicals were purchased from Sinopharm Chemical Reagent Co., Ltd. and Shanghai Macklin Biochemical Co., Ltd. Beyond that, all the reagents were of analytical grade or higher and were used without further purification.

2.2. Catalyst preparations

Typically, Dicyandiamide (DCD, 6.7 g) were dissolved in deionized water; activated carbon powder (AC, 6.7 g) was added to the above solution. Then, the suspension was stirred at 50 °C until the bulk water evaporated completely, and the obtained solid was further dried at 120 °C for 1 h. Subsequently, the solid mixture was transferred into a covered ceramic crucible (semi-closed state). Then the crucible filled with catalyst precursor was calcined at 550 °C for 1.5 h at a ramp rate of 5 °C/min in static air and N_2 flow, respectively. After naturally cooling down to room temperature, the desired products were obtained, which was named g-C_3N_4 @AC-A and g-C_3N_4 @AC-N, here A and N represented air and nitrogen atmosphere, respectively.

In addition, in order to study catalytic mechanism, pure g-C_3N_4-A and g-C_3N_4-N were prepared by the above method in the absence of AC.

2.3. Characterizations

Powder X-ray radiation diffraction (XRD) was recorded on a Rigaku Utima IV (Cu Kα radiation, $\lambda = 0.154178$ nm). The textural properties of the as-prepared catalyst samples were collected on the ASAP 2460 instrument at 77 K; the specific surface area was calculated using the Brunauer-EmmettTeller (BET) method; the pore volume and pore size distribution were obtained using the Barrett-Joyner-Halenda (BJH) method. The determination of elements of the catalysts samples was performed by X-ray Photoelectron Spectroscopy (XPS) (Thermo Fisher ESCALAB Xi+). Fourier Transform Infrared Measurement (FT-IR) was carried out using Nicolet iS50 spectrometer. The electron paramagnetic resonance spectra (ESR) of the catalyst samples were determined using Bruker EMXplus spectrometer. The Raman spectra were obtained on Thermo Fisher DXR2 spectrometer. A scanning electron microscope (SEM) (Hitachi S-4800) was used for the morphology and transmission electron microscopy imagines (TEM) were obtained on FEI talos F200X.

2.4. Typical procedure for the one-pot reductive N-formylation of nitro compounds to N-formamides

The one-pot reductive N-formylation of nitro compounds to N-formamides was carried out in a stainless steel teflon-lined autoclave reactor (50 mL). In a typical reaction procedure, nitro compounds (5 mmol), formic acid (40 mmol), sodium formate (10 mmol) and the catalyst (0.3 g) were added to the autoclave reactor. Before the reaction started, the autoclave was purged with argon gas and sealed under normal pressure. The mixture was vigorously agitated by a magnetic stirrer at 120 °C for a given period of time. After the completion of the reaction, the reactor was cooled to room temperature. Ethyl acetate was added (10 mL) to the reaction mixture and stirred at 60 °C for half an hour. Then filtration was conducted to separate the solid catalyst, and the obtain residue was washed by ethyl acetate to completely extract the organic compound. The ethyl acetate extract mixtures were collected together and analyzed by using Agilent GC-MS 7890 and Shimadzu GC-2010 Plus with a FID detector (Dodecane as a GC internal standard). The reaction products were confirmed by GC-MS as well as by comparing the retention times of standard substances in GC traces.

3. Results and discussion

3.1. Optimization of reaction conditions

The one-pot reductive formylation reaction of nitrobenzene and FA was selected as the model reaction to optimize the catalytic system and reaction conditions (Table 1). In the initial research, based on our study accumulation in N-doping carbon based transition metal catalyst [36–38], Co-N-C and Cu-N-C composite supported on AC were prepared for the formylation reaction. It was found that the metal badly leached from catalyst in acidic environment although protective structures (metal particle encapsulated in CNT and coated by carbon layer) were formed in these catalysts (seeing references 36–38). Associating with the fact that metal-free nitrogen-carbon composites possessed hydrogenation property[39,40], we attempted to prepare a g-C_3N_4 supported on activated carbon without any metal by the pyrolysis process in nitrogen (g-C_3N_4 @AC-N) for this transformation. And an amide yield of 28% was obtained, which demonstrated that metal-free nitrogen-carbon composite had encouraging potential (Entry 1, Table 1). The previous studies revealed that the introduction of $HCOO^-$ facilitated the dehydrogenation rather than dehydration and avoided the O-H cleavage step with high activation energy requirement, so the hydrogen production rate was higher in a mixture of FA and SF than FA-only [41,42]. From this, FA-SF mixed system was employed instead of FA to speed the formylation reaction of nitrobenzene. As expected, the introduction of SF distinctly stimulated the transformation (Entry 2, Table 1). Then the amount of SF was investigated, and the 4:1 molar ratio of FA to SF gave the best result (Entry 3, Table 1). Subsequently, the effect of solvents was also investigated; the desired product could be obtained in solvents. Nevertheless, the best yield was still achieved under solvent-free condition (Table S1).

Furthermore, a g-C_3N_4 supported on activated carbon pyrolyzed in air was tested, and it exhibited higher catalytic activity compared to g-C_3N_4 @AC-N (Entry 1 and 2, Table 2). This illustrated that pyrolysis

Table 1
The effect of SF on the formylation reaction of nitrobenzene with FA a.

Entry	Amount of SF	Amide yields (%)[b]
1	HCOONa (0 mmol)	28
2	HCOONa (5 mmol)	40
3	HCOONa (10 mmol)	46
4	HCOONa (15 mmol)	43

[a]Nitrobenzene (5 mmol), FA(40 mmol), g-C_3N_4 @AC-N (0.3 g), 120 ℃, 4 h, N_2 atmosphere.
[b]GC Yields.

Table 2
Reductive N-formylation of nitrobenzene with FA on various catalysts [a].

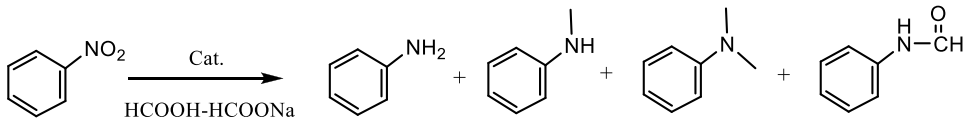

1a 2a 3a 4a 5a

Entry	Catalysts	Reaction conditions	Con. (%)[b]	Selec. (%)[b]				
				2a	3a	4a	5a	others
1	g-C_3N_4@AC-N	120 ℃/4 h	47	0.3	0.2	n.d	98.2	1.3
2	g-C_3N_4@AC-A	120 ℃/4 h	61	0.1	0.3	n.d	98.5	1.1
3	g-C_3N_4-N	120 ℃/4 h	10	1.8	2.0	0.5	92.5	3.2
4	g-C_3N_4-A	120 ℃/4 h	16	1.1	2.9	1.3	91.7	3.0
5	g-C_3N_4@AC-A	130 ℃/10 h	99	n.d	0.6	0.2	99.0	0.2
6	—	120 ℃/4 h	4	1.5	n.d	n.d	76.1	22.4

[a] Reaction conditions: nitrobenzene (5 mmol), FA (40 mmol), SF (10 mmol), catalyst (0.3 g), N_2 atmosphere.
[b] GC results

atmosphere had important role on catalytic behavior of catalyst. The corresponding g-C_3N_4-N and g-C_3N_4-A samples without support were also prepared and examined, and similar results were obtained. The catalytic performance of g-C_3N_4-A was better than that of g-C_3N_4-N (Entry 3 and 4, Table 2). And, the activities of two pure g-C_3N_4 samples were much lower compared with the corresponding supported, which manifested that the support AC had significant influence on catalytic performance. In order to completely achieve the transformation, we raised reaction temperature and prolonged reaction time, and a 98% yield of formamide was acquired (Entry 5, Table 2). Additionally, an experiment was also carried out in the absence of catalyst; only a small amount of formamide was obtained (Entry 6, Table 2). The blank experiment proved the effectiveness of these metal-free nitrogen-carbon composites.

3.2. *Structure characterization and catalytic mechanism of nitrogen-carbon composites*

To understand the catalytic properties of nitrogen-carbon composites and reveal the catalytic mechanism involved, the morphology and microstructure of pure g-C_3N_4 samples in different pyrolysis atmosphere were observed by SEM and TEM. It could be seen from SEM images in Fig. 1(a) and (d) that pure g-C_3N_4 samples displayed bulk morphology of agglomerates with nano-and micro-pores on the surface. g-C_3N_4-A had

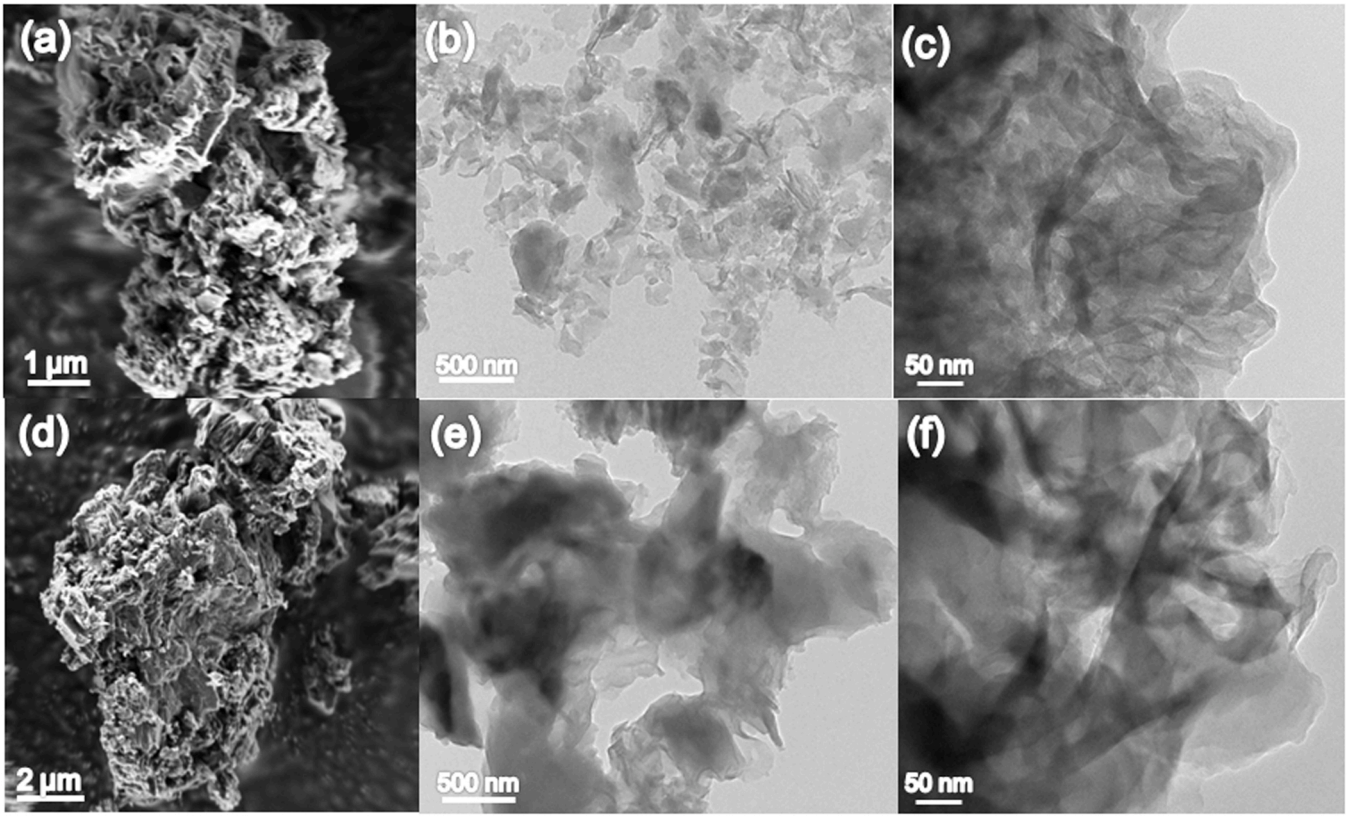

Fig. 1. The morphology and microstructure characterization of pure g-C_3N_4 samples: (a) SEM image of g-C_3N_4 -A, (b) (c) TEM images of g-C_3N_4-A; (d) SEM image of g-C_3N_4-N, (e) (f) TEM images of g-C_3N_4-N.

more pores and looser morphology than g-C_3N_4-N. TEM micrographs also supported it (seeing Fig. 1(b) and (e)). Moreover, thinner sheets and wrinkles with roughness or grain boundaries were presented in g-C_3N_4-A in Fig. 1(c) and (f), hereby creating more edges and defects which improved the performance of the catalyst.

Next, XRD was performed to characterize the crystalline structures of the catalysts. Fig. 2 showed the XRD patterns of various catalyst samples. For pure g-C_3N_4, two significant characteristic peaks of g-C_3N_4 at around 13.5° and 27.5°, assigned to the (100) and (002) planes, were observed [43,44]. XRD patterns of the two supported g-C_3N_4 samples only displayed two broad peaks, no characteristic peaks of g-C_3N_4 were found. Combined with XRD pattern of AC, the peak centered at 43.2° could be attributed to the (101) planes of AC, whereas the peak centered at 23.9° should be a joint result of 27.5° peak of g-C_3N_4 and 21.6° of AC support. The analyses demonstrated that g-C_3N_4 was formed in the supported g-C_3N_4 samples and well dispersed on the support surface, which was one of reason for why the activity of the supported g-C_3N_4 samples were higher than that of pure g-C_3N_4 samples. In-depth analyses showed that pure g-C_3N_4 fired in an air atmosphere than in a N_2 atmosphere the (002) peak shifted to higher angles (from 27.44° to 27.78°), correspondingly interlayer distance decreased from 0.325 nm to 0.321 nm (Table S2). And, the intensity of diffraction peaks of g-C_3N_4-A was slightly stronger than that of g-C_3N_4-N demonstrating that the crystallite size increased, which seemed not to support the activity test results because the smaller crystallite size generally possessed higher catalytic activity. Thus, XPS was carried out to gain more details on the structure and composition of the as-prepared catalysts.

The full XPS survey spectra indicated the samples were mainly made up of C, N, and O elements (Fig. S1). Correspondingly, the atom ratios of carbon to nitrogen ($R_{C:N}$) of g-C_3N_4-N and g-C_3N_4-A were calculated to be 0.89 and 0.84 (Table S3), respectively, which showed that greater carbon loss occurred in air atmosphere calcination. Previous work suggested that such variation of C/N ratio meant the generation of carbon defect sites [45–47]. Meanwhile, defect as catalytic site had been widely investigated and accepted in catalysis [48,49]. It was therefore reasonable to conjecture that there were more richly available carbon defects on the surface of g-C_3N_4-A prepared in this study than g-C_3N_4-N. To understand this proposed carbon defect formation, the resolutions of element spectrum peaks of g-C_3N_4-A and g-C_3N_4-N were carefully conducted to analyze the difference of chemical state of elements. As shown in Fig. 2, XPS spectra of g-C_3N_4-A and g-C_3N_4-N could be deconvoluted into four peaks at 284.5, 286.1, 287.9 eV and 288.7 eV, which ascribed to adventitious carbon, the carbon in C-NH_x groups, tertiary carbon C_3N and =CNH_2 groups, denoted as C_1, C_2, C_3, and C_4, respectively [50,51], demonstrating that these two samples maintained a basic tri-s-triazine structure. Meanwhile, the C_3 ratio in the whole carbon decreased from 0.68 of g-C_3N_4-N to 0.65 of g-C_3N_4-A (Table S4), which suggested the missing of carbon moiety and formation of more carbon defects at the tertiary carbon sites [50]. Additionally, the previous studies indicated that the content of amino groups was positively related to the carbon defect at tertiary carbon and the ratio of C_3 to C_4 implied the changed concentration of amino groups to some extent [52–54]. In our case, g-C_3N_4-A showed the lower ratio of C_3/C_4 compared with the counterpart (5.42 vs 7.56, Table S4), which represented a higher the content of amino groups, further manifesting the higher concentration of carbon defects in g-C_3N_4-A. The N 1 s spectra of the samples also could confirm this issue. Four main peaks at 398.5, 399.7, 400.9, and 404.0 eV, assigned to sp^2-hybridized C=N–C structure (N_1), tertiary nitrogen N-$(C)_3$ (N_2), –NH_x groups (N_3) and π excitation effect in heptazine rings (N_4), respectively, were identified in the N 1 s spectra (Fig. 2) [55,56]. The report pointed out that the ratio of N_3/N_2 had a positive relation with the number of amino groups [57], while the higher content of amino groups signified more carbon defects, so g-C_3N_4-A with the bigger ratio value of N_3/N_2 (0.83 vs 0.61) had higher content of carbon defects (Table S5) [53,57,58]. Note that the presence of amino groups generated hydrogen-bonding interaction between g-C_3N_4 layers to result in the decrease of the distance between interlayer [58]. Therefore, g-C_3N_4-A containing larger number of amino groups exhibited the smaller interlayer distance, which corresponded with the XRD results. To further confirm carbon defects, EPR was used to detect the formation of surface defects.

Fig. 3a depicted ESR spectra of pure g-C_3N_4-N and g-C_3N_4-A. As observed, two samples exhibit a major ESR signal with g value of 2.004, ascribed to unpaired electrons on carbon atoms of the heptazine rings. Compared with g-C_3N_4-N, the ESR signal intensity of g-C_3N_4-A attenuated, which demonstrated the less of carbon content in its structure, further indicating the formation of carbon vacancies in g-C_3N_4-A samples [47,52,59]. Subsequently, the surface groups on samples were

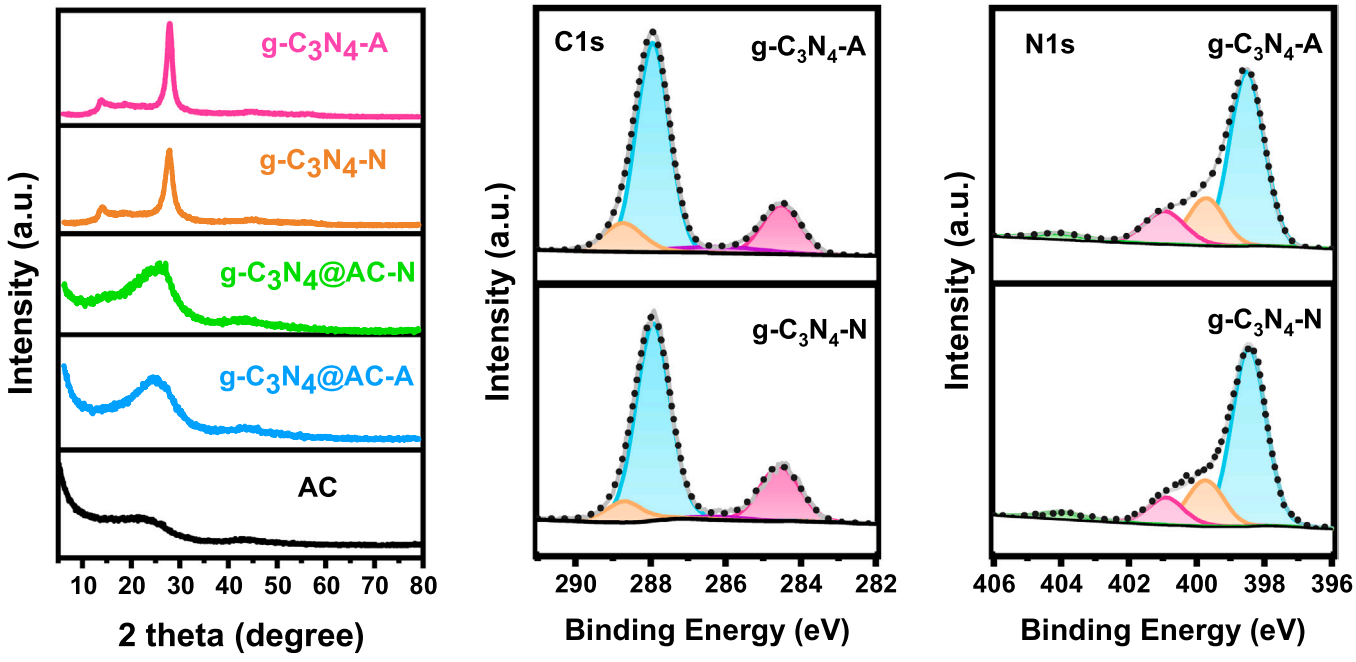

Fig. 2. XRD patterns of various catalyst samples and XPS spectra of pure g-C_3N_4-N and g-C_3N_4-A.

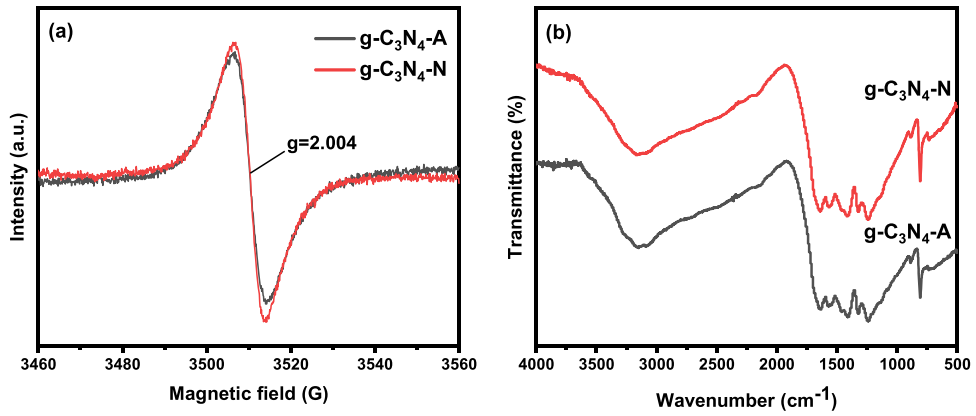

Fig. 3. (a) EPR and (b) FT-IR spectra of pure g-C_3N_4-N and g-C_3N_4-A samples.

determined by FT-IR spectra (Fig. 3b). The sharp peak at 808 cm^{-1} of g-C_3N_4-A, assigned to the C-N stretching vibration of the characteristic tri-s-triazine structure, was weaker than that of g-C_3N_4-N (Fig. 3b), manifesting the appearance of more carbon vacancies since carbon vacancies destroyed the structural integrity of the tri-s-triazine structure [60,61]. In addition, FT-IR spectra in Fig. S2 showed that the main absorption peaks of g-C_3N_4-A and AC appeared in the spectra of g-C_3N_4@AC-A implying the interfacial interaction between g-C_3N_4-A and AC, which corresponded with XRD. This would induce the improvement of the catalytic efficiency.

Raman spectroscopy was a common method to characterize the defect of carbon materials. As we knew, the ratio of D band with G band (I_D/I_G) was related with the defective content of carbon materials [62,63]. It could see from the Raman spectra of g-C_3N_4@AC-N and g-C_3N_4@AC-A in Fig. 4 that the I_D/I_G value of g-C_3N_4@AC-A was bigger than that of g-C_3N_4@AC-N (5.33 vs 3.61), representing the more carbon defects in g-C_3N_4@AC-A.

As for the issue that the crystallite size from XRD did not support the activity test results for pure g-C_3N_4, we thought that the crystallite size was one of factors affecting catalytic activity and did not dominate the catalytic behavior. Taking the SEM, TEM, XRD, XPS, FT-IR, EPR and Raman spectrum together, it could be concluded that carbon defect in g-C_3N_4 was responsible for the difference in the catalytic activity of g-C_3N_4-A and g-C_3N_4-N and air atmosphere more favored the formation of carbon defect.

Furthermore, the textural properties of various catalysts were investigated by N_2 adsorption-desorption method. As shown in Fig. 5,

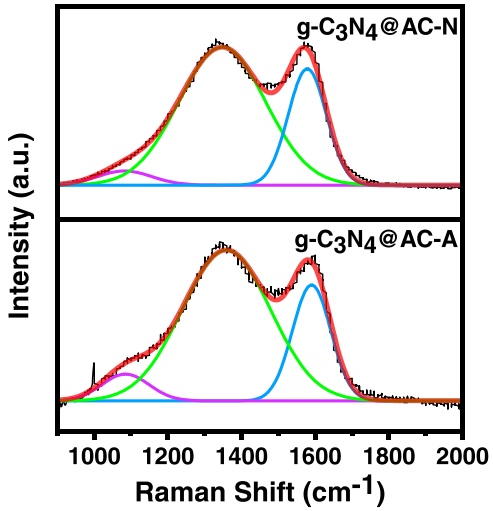

Fig. 4. Raman spectra of g-C_3N_4@AC-N and g-C_3N_4@AC-A.

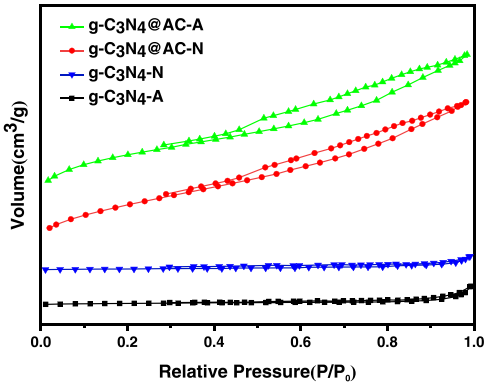

Fig. 5. N_2 adsorption/desorption isotherms of different catalyst samples.

the isotherms of all the samples displayed a type IV-like isotherm curve with hysteresis loop, indicative of mesoporous materials. Obviously, the supported g-C_3N_4 catalysts possessed more developed pore system relative to pure g-C_3N_4 catalysts (Table 3), which demonstrated that the support AC was able to well disperse g-C_3N_4 (this was also supported by XRD characterization), thereby gaining the higher catalytic performance. And, the specific area and pore volume of g-C_3N_4 @AC-A were much bigger than those of g-C_3N_4 @AC-N. This suggested that the pyrolysis in air atmosphere could obtain more developed pore organization, which benefited catalytic performance.

3.3. The exploration of the universality of our procedure

With the optimized conditions in hand, the universality of our procedure was investigated using a wide range of structurally diverse nitrobenzenes and FA as starting materials. The results were summarized

Table 3
The textural properties of the as-prepared catalyst samples.

Sample	Specific surface area (m^2/g)	Pore volume (cm^3/g)	Mean pore size (nm)
g-C_3N_4-N	11.0	0.26	3.6
g-C_3N_4-A	11.4	0.35	4.0
g-C_3N_4@AC-N	275.6	0.30	4.0
g-C_3N_4@AC-A	499.6	0.40	4.1

According to the above analysis and appraisal, the high catalytic property of g-C_3N_4 @AC-A could be ascribed to carbon defect and the dispersion effect of the support AC. Pyrolysis in air atmosphere obtained more carbon defects and the support AC effectively dispersed g-C_3N_4 to expose more active sites.

Table 4
One-pot reductive formylation reactions of nitro compounds and FA catalyzed by g-C_3N_4@AC-A[a].

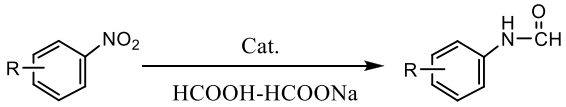

1 5

Entry	Substrates	Reaction times (h)	Yields of 5 (%)[b]
1	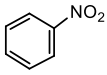	10	98
2	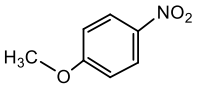	16	94
3	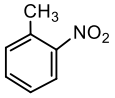	14	94
4	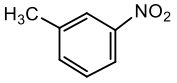	14	95
5	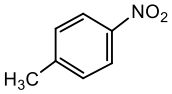	14	99
6	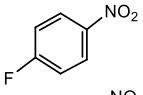	14	96
7	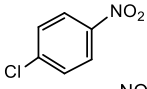	14	98
8	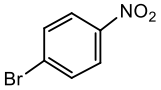	16	86
9	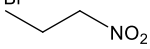	16	72
10[c]	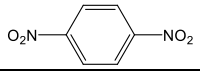	20	28

[a]Reaction conditions: nitro compounds (5 mmol), FA (40 mmol), SF (10 mmol), g-C_3N_4@AC-A (0.3 g), 130 ℃, N_2 atmosphere.
[b] GC Yields.
[c] Yield of N-(4-Formamidophenyl) formamide.

in Table 4. Overall, our protocol enabled the N-formylation of nitro aromatics containing both electron-donating (–Me, –OMe) and electron-withdrawing groups (–F, –Cl, and –Br) into the corresponding amides in good yields. The reactions of regioisomers of methylnitrobenzene with FA were investigated; a weak effect of steric hindrance was observed (Entry 3–5, Table 4). Moreover, dehalogenation was not found for halogenated nitrobenzenes, generally occurring in catalytic hydrogenation process. Aliphatic nitro compound nitropropane was also tested; its reactivity was noticeably lower than nitroarenes (Entry 9, Table 4). Additionally, for *p*-dinitrobenzene transformation, multiple products were formed based on GC-MS (such as *p*-nitroaniline, diphenylamine, *p*-aminobenzamide), only 28% yield of N-(4-Formamidophenyl) formamide was obtained under our given condition.

3.4. The reusability of the g-C_3N_4@AC-A catalyst

We explored the reusability of the g-C_3N_4@AC-A catalyst by the reductive formylation reaction of nitrobenzene and FA as the probe reaction. Prior to reuse in the next run, the catalyst needed to be washed using water and ethyl acetate orderly twice under ultrasound irradiation. The test reactions were performed under our optimized condition. It could be seen from Fig. 6 that catalytic activity could be maintained during the first four rounds (from 98% to 95%) and a small activity loss was found in five rounds (90%); while we extended the reaction time to 12 h, a satisfactory yield was given (98%).

In order to explore the cause of recycled catalyst deactivation, we performed SEM, XRD, N_2 adsorption/ desorption, XPS and Raman spectroscopy characterization for the spent catalyst after 5 cycles (Fig. 7). SEM imagines of both the fresh and spent catalyst displayed numerous small particles on the substrate AC. No significant change was observed from SEM. XRD of the spent catalyst exhibited two broad peaks centered at 43.2° and 23.9°, which was similar to that of fresh catalyst. N_2 adsorption/desorption showed that the specific surface area and pore volume of the spent catalyst decreased compared to the fresh catalyst (seeing Fig. 7d). The main reason for this, we thought, was that reagent-(nitrobenzene, FA) and product (e.g. N-pheny formamide) were adsorbed on the surface of catalyst, resulting in a decrease in the developed degree of pore organization. The full spectrum of XPS in Fig. 7e displayed that the content of N decreased and the content of O increased relative to the fresh catalyst after catalyst was reused, which supported the attachment of the reagent and product to the catalyst. Moreover, the I_D/I_G value from Raman spectrum decreased (from 5.33 of the fresh catalyst to 3.95 of the spent catalyst) (Fig. 7f), meaning the decrease of carbon defects in spent catalyst.

In a word, the cause of recycled catalyst deactivation should be that the attachment of the organics covered the active site, leading to the decline of catalytic performance according to above characterization.

To show the benefits and disadvantages of our procedure, we summarize the literature results for the reductive N-formylation of nitrobenzene. It can be seen in Table 5 that the advantage of our protocol is metal-free catalyst and solvent-free condition. g-C_3N_4 @AC-A settles the high cost and metal leaching of metal catalyst. And, solvent-free reaction condition met the requirements of green chemistry. The catalytic performance and the universality for structurally diverse nitro compounds of our catalyst need to been improved. Thus, the following work is to further enhance catalytic performance of metal-free C-N composite and optimize reaction procedure to obtain the higher practicability.

4. Conclusion

An efficient, low cost and metal-free g-C_3N_4@AC-A catalyst was developed for one-pot reductive N-formylation of nitro compounds and sodium formate was introduced to speed up this reaction. Benefited of these, a broad set of nitro compounds were successfully converted to their corresponding formamides in good to high yields with various functional group tolerances under the solvent-free condition. Metal-free catalyst avoided the leaching of metal and metal pollution of product fundamentally. The catalyst could be recovered and recycled several times without marked loss of activity. Based on the instrument analyses, the high catalytic property of g-C_3N_4@AC-A could be ascribed to carbon

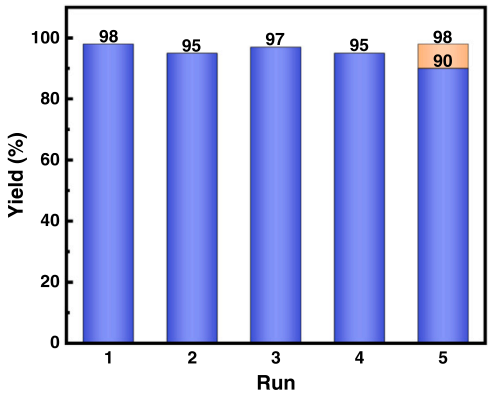

Fig. 6. Reusability of the g-C_3N_4@AC-A catalyst.

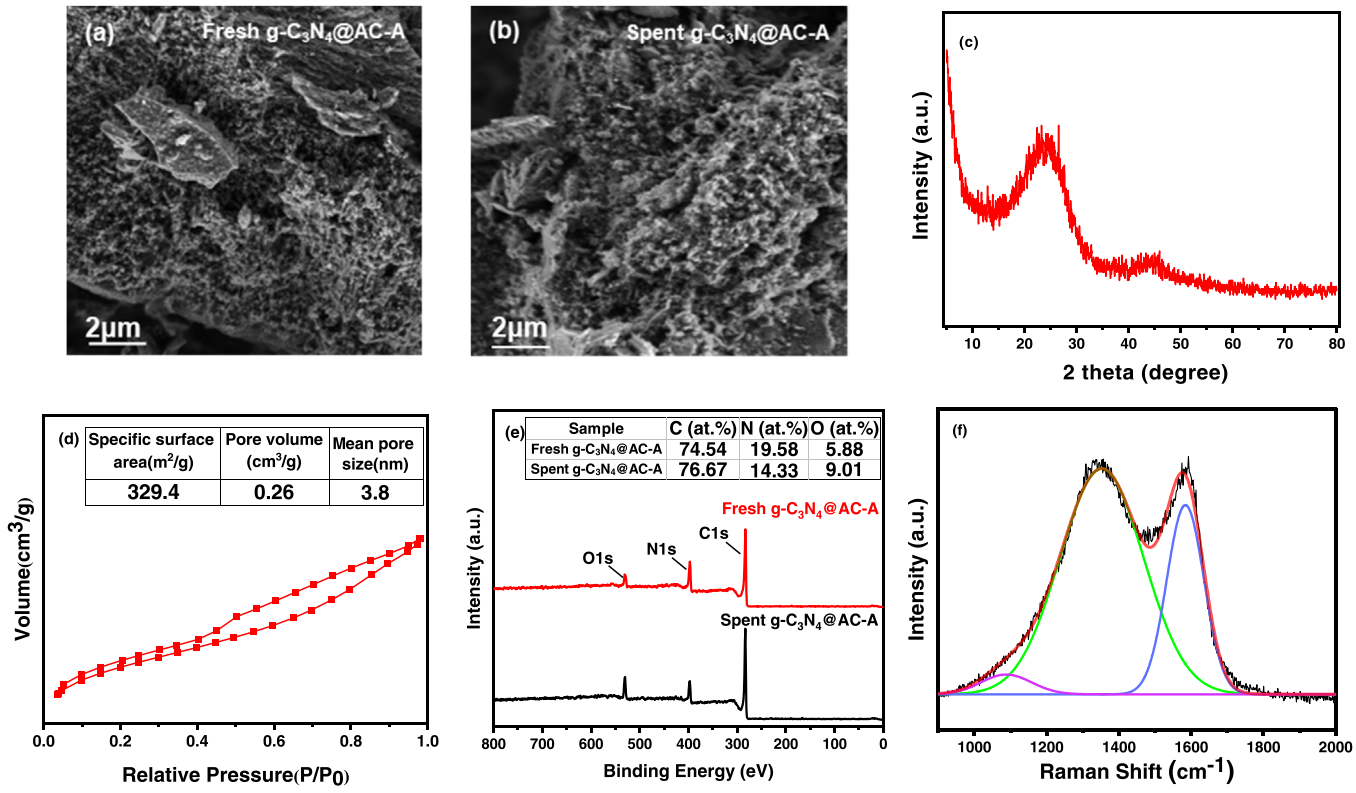

Fig. 7. SEM, XRD, N_2 adsorption/desorption, XPS and Raman spectrum of spent g-C_3N_4@AC-A catalyst.

Table 5
Comparison of various procedures for N- formylation of nitrobenzene.

Entry	Catalyst	Reaction condition	Yields (%)	References
1	AgPd@g-C_3N_4	Nitrobenzene (1 mmol); FA (2 mmol); catalyst (25 mg); water (1.0 mL); 40 watt domestic bulb; 2 h.	99	[16]
2	Au/rutile	Nitrobenzene (1 mmol); FA (4 mmol);Au (1 mol%); toluene(5 mL); N_2 (1 bar); 70 °C; 2 h.	96	[17]
3	Mag-IL-Pd	Nitrobenzene (0.25 mmol); FA (30equiv); catalyst (0.25 mol %); water (1 mL); Ar; 90 °C;24 h.	97	[15]
4	CoNC-700	Nitrobenzene (0.5 mmol); FA (5 mmol); catalyst 9.5 mg (1 mol% Co); acetonitrile (5 mL); N_2(1 bar); 110 °C; 6 h.	96	[19]
5	ZnNC-1000	Nitrobenzene (0.5 mmol); FA (6 equiv); catalyst(20 mg); THF (2 mL); Ar; 150 °C; 16 h.	96	[22]
6	ZnCo-N@$C_{(ZIF\text{-}COF)}$	Nitrobenzene (1 mmol); FA (12 equiv); catalyst(30 mg); THF (7 mL); 200 °C; 8 h.	85	[21]
7	Co@NSC-800	Nitrobenzene (0.5 mmol); FA (14 equiv); catalyst (20 mg); water (3 mL); 110 °C; 5 h.	96	[20]
8	$[Cp^*RhCl_2]_2$	Nitrobenzene (1.6 mmol); FA (32 mmol); catalyst (0.1 mol %); KI(1.6 mmol); DMSO (2 mL); Et_3N (10.7 mmol); Ar; 100 °C; 20 h	69	[18]
9	g-C_3N_4@AC-A	Nitrobenzene (5 mmol); FA (40 mmol), SF (10 mmol); catalyst (0.3 g); N_2;130 °C; 10 h.	98	This work

defect and the dispersion effect of the support AC. Air pyrolysis obtained more carbon defect and the support AC effectively dispersed g-C_3N_4 and exposed more active sites. In summary, this study provided a green, efficient and practical methodology for the expedient synthesis of formamides from nitro compounds.

CRediT authorship contribution statement

Xing Wang: Validation, Formal analysis, Investigation, Data curation, Writing – original draft, Writing – review & editing. **Xiaona Liu**: Methodology, Validation, Data curation. **Hui Wen**: Validation, Formal analysis. **Kai Guo**: Formal analysis, Visualization. **Hlomayi Brendon**: Visualization, Writing – review & editing. **Di Liu**: Investigation, Conceptualization, Methodology, Resources, Supervision, Project administration, Funding acquisition, Writing – review & editing.

Declaration of Competing Interest

The authors declare that they have no known competing financial interests or personal relationships that could have appeared to influence the work reported in this paper.

Data availability

Data will be made available on request.

Acknowledgements

This work was supported by Open Foundation of Hubei Key Laboratory of Processing and Application of Catalytic Materials (Grant No. 202203604) and Natural Science Foundation of Shandong Province, China (Grant No. ZR2020KE035).

Appendix A. Supporting information

Supplementary data associated with this article can be found in the online version at doi:10.1016/j.apcatb.2022.122042.

References

[1] D.G. Brown, J. Bostrom, Analysis of past and present synthetic methodologies on medicinal chemistry: where have all the new reactions gone? J. Med. Chem. 59 (10) (2016) 4443–4458.

[2] R. Dong, S. Clark, L. Laouar, L. Heinrichs, K. Wu, N.M. Jomha, J.A.W. Elliott, Evaluation of the permeation kinetics of formamide in porcine articular cartilage, Cryobiology (2022), https://doi.org/10.1016/j.cryobiol.2022.05.002.

[3] H. Bipp, H. Kieczka, In Ullmann's Encyclopedia of Industrial Chemistry, Wiley-VCH, Weinheim, Germany, 2003, pp. 36–47.

[4] Y. Ma, Q. Zhang, L. Liu, Y. Li, H. Li, Z. Yan, J. Chen, N, N-dimethylformamide tailors solvent effect to boost Zn anode reversibility in aqueous electrolyte, Natl. Sci. Rev. (2022), https://doi.org/10.1093/nsr/nwac051.

[5] P.H. Huy, Formamide catalysis facilitates the transformation of aldehydes into geminal dichlorides, Synthesis 51 (12) (2019) 2474–2483.

[6] S. Yang, A. Cho, J.H. Cho, B.M. Kim, Oxidative N-formylation of secondary amines catalyzed by reusable bimetallic AuPd-Fe3O4 nanoparticles, Nanomaterials 11 (8) (2021), 103390.

[7] M.C. Pichardo, G. Tavakoli, J.E. Armstrong, T. Wilczek, B.E. Thomas, M.H. G. Prechtl, Copper-catalyzed formylation of amines by using methanol as the C1 source, Chemsuschem 13 (5) (2020) 882–887.

[8] D. Dan, F. Chen, W. Zhao, H. Yu, S. Han, Y. Wei, Chromium-catalysed efficient N-formylation of amines with a recyclable polyoxometalate-supported green catalyst, Dalton Trans. 50 (1) (2021) 90–94.

[9] D. Habibi, M. Nasrollahzadeh, H. Sahebekhtiari, Green synthesis of formamides using the Natrolite zeolite as a natural, efficient and recyclable catalyst, J. Mol. Catal. A Chem. 378 (2013) 148–155.

[10] M. Nasrollahzadeh, N.S.S. Bidgoli, B.G.M. Rocha, A.J.L. Pombeiro, K. T. Mahmudov, N-Formylation of amines using arylhydrazones of malononitrile and a Cu(II) complex under eco-friendly conditions at room temperature, Inorg. Chim. Acta 513 (2020), 119938.

[11] M. Nasrollahzadeh, S.M. Sajadi, A. Hatamifard, Anthemis xylopoda flowers aqueous extract assisted in situ green synthesis of Cu nanoparticles supported on natural Natrolite zeolite for N-formylation of amines at room temperature under environmentally benign reaction conditions, J. Colloid Interface Sci. 460 (2015) 146–153.

[12] M. Nasrollahzadeh, N.S.S. Bidgoli, M.M. Karimkhani, Valorization of lignin: antibacterial and catalytic activities of copper complex stabilized on magnetic lignosulfonate for N-formylation of amines under solvent-free conditions, Biomass Convers. Biorefin. (2021), https://doi.org/10.1007/s13399-021-01841-y.

[13] O. Saidi, M.J. Bamford, A.J. Blacker, J. Lynch, S.P. Marsden, P. Plucinski, R. J. Watson, J.M.J. Williams, Iridium-catalyzed formylation of amines with paraformaldehyde, Tetrahedron Lett. 51 (44) (2010) 5804–5806.

[14] M. Nasrollahzadeh, N. Motahharifar, M. Sajjadi, A.M. Aghbolagh, M. Shokouhimehr, R.S. Varma, Recent advances in N-formylation of amines and nitroarenes using efficient (nano)catalysts in eco-friendly media, Green Chem. 21 (19) (2019) 5144–5167.

[15] B. Karimi, F. Mansouri, H. Vali, A highly water-dispersible/magnetically separable palladium catalyst: selective transfer hydrogenation or direct reductive N-formylation of nitroarenes in water, Chempluschem 80 (12) (2015) 1750–1759.

[16] R.B.N. Baig, S. Verma, M.N. Nadagouda, R.S. Varma, A photoactive bimetallic framework for direct aminoformylation of nitroarenes, Green Chem. 18 (4) (2016) 1019–1022.

[17] L. Yu, Q. Zhang, S. Li, J. Huang, Y. Liu, H. He, Y. Cao, Gold-catalyzed reductive transformation of nitro compounds using formic acid: mild, efficient, and versatile, ChemSusChem 8 (18) (2015), 101002.

[18] Y. Wei, J. Wu, D. Xue, C. Wang, Z. Liu, Z. Zhang, G. Chen, J. Xiao, Highly efficient rhodium-catalyzed transfer hydrogenation of nitroarenes into amines and formanilides, Synlett 25 (9) (2014) 1295–1298.

[19] Y. Zhang, P. Cao, H. Zhang, G. Yin, J. Zhao, Cobalt nanoparticles anchoring on nitrogen doped carbon with excellent performances for transfer hydrogenation of nitrocompounds to primary amines and N-substituted formamides with formic acid, Catal. Commun. 129 (2019), 101016.

[20] Q. Zhu, X. Sun, H. Zhao, D. Xu, Z. Dong, Selective transfer hydrogenation and N-formylation of nitroarenes by a facilely prepared N, S co-doped carbon-encapsulated cobalt nanoparticle catalyst, Ind. Eng. Chem. Res. 59 (13) (2020) 5615–5623.

[21] A.K. Kar, R. Srivastava, Reductive formylation of nitroarenes using HCOOH over bimetallic C-N framework derived from the integration of MOF and COF, Chemcatchem 13 (13) (2021) 3174–3183.

[22] J. Li, C. Li, S. Feng, Z. Zhao, H. Zhu, Y. Ding, Atomically dispersed Zn-N_x sites in N-doped carbon for reductive n-formylation of nitroarenes with formic acid, ChemCatChem 12 (6) (2020) 1546–1550.

[23] V. Sanko, A. Senocak, S.O. Tumay, Y. Orooji, E. Demirbas, A. Khataee, An electrochemical sensor for detection of trace-level endocrine disruptor bisphenol A using Mo2Ti2AlC3 MAX phase/MWCNT composite modified electrode, Environ. Res. 212 (2022), 113071.

[24] S. Arefi-Oskoui, A. Khataee, S.J. Behrouz, V. Vatanpour, S.H. Gharamaleki, Y. Orooji, M. Safarpour, Development of MoS2/O-MWCNTs/PES blended membrane for efficient removal of dyes, antibiotic, and protein, Sep. Purif. Technol. 280 (2022), 119822.

[25] K.M. Yam, N. Guo, Z. Jiang, S. Li, C. Zhang, Graphene-based heterogeneous catalysis: role of graphene, Catalysts 10 (1) (2020) 53.

[26] F. Besharat, F. Ahmadpoor, Z. Nezafat, M. Nasrollahzadeh, N.R. Manwar, P. Fornasiero, M.B. Gawande, Advances in carbon nitride-based materials and their electrocatalytic applications, ACS Catal. 12 (9) (2022) 5605–5660.

[27] Y. Orooji, M. Ghanbari, O. Amiri, M. Salavati-Niasari, Facile fabrication of silver iodide/graphitic carbon nitride nanocomposites by notable photo-catalytic performance through sunlight and antimicrobial activity, J. Hazard. Mater. 389 (2020), 122079.

[28] G. Liao, Y. Gong, L. Zhang, H. Gao, G. Yang, B. Fang, Semiconductor polymeric graphitic carbon nitride photocatalysts: the "holy grail" for the photocatalytic hydrogen evolution reaction under visible light, Energy Environ. Sci. 12 (7) (2019) 2080–2147.

[29] W.J. Ong, L.L. Tan, Y.H. Ng, S.T. Yong, S.P. Chai, Graphitic carbon nitride (g-C_3N_4)-based photocatalysts for artificial photosynthesis and environmental remediation: are we a step closer to achieving sustainability? Chem. Rev. 116 (12) (2016) 7159–7329.

[30] F. Jia, X. Peng, L. Jiang, X. Yuan, X. Chen, Y. Zhao, W. Zhang, Recent advances in graphitic carbon nitride as a catalyst for heterogeneous Fenton-like reactions, Dalton Trans. 50 (46) (2021) 16887–16908.

[31] A. Nasri, B. Jaleh, Z. Nezafat, M. Nasrollahzadeh, S. Azizian, H.W. Jang, M. Shokouhimehr, Fabrication of g-C3N4/Au nanocomposite using laser ablation and its application as an effective catalyst in the reduction of organic pollutants in water, Ceram. Int. 47 (3) (2021) 3565–3572.

[32] A. Nasri, B. Jaleh, S. Khazalpour, M. Nasrollahzadeh, M. Shokouhimehr, Facile synthesis of graphitic carbon nitride/chitosan/Au nanocomposite: a catalyst for electrochemical hydrogen evolution, Int. J. Biol. Macromol. 164 (2020) 3012–3024.

[33] F. Goettmann, A. Fischer, M. Antonietti, A. Thomas, Chemical synthesis of mesoporous carbon nitrides using hard templates and their use as a metal-free catalyst for Friedel-Crafts reaction of benzene, Angew. Chem. Int. Ed. 45 (27) (2006) 4467–4471.

[34] P. Choudhary, A. Sen, A. Kumar, S. Dhingra, C.M. Nagaraja, V. Krishnan, Sulfonic acid functionalized graphitic carbon nitride as solid acid-base bifunctional catalyst for Knoevenagel condensation and multicomponent tandem reactions, Mater. Chem. Front. 5 (16) (2021) 6265–6278.

[35] X. Li, Y. Wang, L. Kang, M. Zhu, B. Dai, A novel, non-metallic graphitic carbon nitride catalyst for acetylene hydrochlorination, J. Catal. 311 (2014) 288–294.

[36] D. Liu, P. Yang, H. Zhang, M. Liu, W. Zhang, D. Xu, J. Gao, Direct reductive coupling of nitroarenes and alcohols catalysed by Co–N–C/CNT@ AC, Green Chem. 21 (8) (2019) 2129–2137.

[37] C. Zhang, P. Zhao, Z. Zhang, J. Zhang, P. Yang, P. Gao, J. Gao, D. Liu, Co-N-C supported on SiO_2: a facile, efficient catalyst for aerobic oxidation of amines to imines, RSC Adv. 7 (75) (2017) 47366–47372.

[38] M. Liu, H. Zhang, J. Wang, G. Zhao, D. Liu, Mechanisms; catalysis, relationship between the structure and dehydrogenation of alcohols/hydrogenation of nitroarenes and base catalysis performance of Co-N-C catalyst, React. Kinet. Mech. Catal. 129 (2) (2020) 865–881.

[39] W. Xiong, Z. Wang, S. He, F. Hao, Y. Yang, Y. Lv, W. Zhang, P. Liu, H. Luo, Nitrogen-doped carbon nanotubes as a highly active metal-free catalyst for nitrobenzene hydrogenation, Appl. Catal. B Environ. 260 (2020), 118105.

[40] A. Primo, A. Rendón-Patiño, C. Bucur, A. Jurca, B. Cojocaru, V.I. Parvulescu, H. Garcia, Doped microporous graphitic carbons as metal-free catalysts for the selective hydrogenation of alkynes to alkenes, J. Catal. 405 (2022) 355–362.

[41] M. Yurderi, A. Bulut, M. Zahmakiran, M. Kaya, Carbon supported trimetallic PdNiAg nanoparticles as highly active, selective and reusable catalyst in the formic acid decomposition, Appl. Catal. B Environ. 160 (2014) 514–524.

[42] H. Zhong, M. Iguchi, M. Chatterjee, Y. Himeda, Q. Xu, H. Kawanami, Formic acid-based liquid organic hydrogen carrier system with heterogeneous catalysts, Adv. Sustain. Syst. 2 (2) (2018) 1700161.

[43] I. Papailias, N. Todorova, T. Giannakopoulou, N. Ioannidis, P. Dallas, D. Dimotikali, C. Trapalis, Novel torus shaped g-C3N4 photocatalysts, Appl. Catal. B Environ. 268 (2020), 118733.

[44] S. Li, Y. Peng, C. Hu, Z. Chen, Self-assembled synthesis of benzene-ring-grafted g-C_3N_4 nanotubes for enhanced photocatalytic H_2 evolution, Appl. Catal. B Environ. 279 (2020), 119401.

[45] S. Guo, Y. Tang, Y. Xie, C. Tian, Q. Feng, W. Zhou, B. Jiang, P-doped tubular g-C_3N_4 with surface carbon defects: universal synthesis and enhanced visible-light photocatalytic hydrogen production, Appl. Catal. B Environ. 218 (2017) 664–671.

[46] J. Di, J. Xia, X. Li, M. Ji, H. Xu, Z. Chen, H. Li, Constructing confined surface carbon defects in ultrathin graphitic carbon nitride for photocatalytic free radical manipulation, Carbon 107 (2016) 1–10.

[47] Y. Zhang, J. Di, P. Ding, J. Zhao, K. Gu, X. Chen, C. Yan, S. Yin, J. Xia, H. Li, Ultrathin g-C_3N_4 with enriched surface carbon vacancies enables highly efficient photocatalytic nitrogen fixation, J. Colloid Interface Sci. 553 (2019) 530–539.

[48] X. Feng, H.S. Jena, C. Krishnaraj, K. Leus, G. Wang, H. Chen, C. Jia, D.V.P. Van, Generating catalytic sites in UiO-66 through defect engineering, ACS Appl. Mater. Interfaces 13 (51) (2021) 60715–60735.

[49] J. Hong, C. Jin, J. Yuan, Z. Zhang, Atomic defects in two-dimensional materials: from single-atom spectroscopy to functionalities in opto˙/electronics, nanomagnetism, and catalysis, Adv. Mater. 29 (14) (2017) 1606434.

[50] N. Sun, X. Wen, Y. Tan, C. Yan, H. Wang, Generated gas molecules-modified carbon nitride nanosheets with nitrogen vacancies and high efficient photocatalytic hydrogen evolution, Appl. Surf. Sci. 470 (2019) 724–732.

[51] G. Peng, J. Albero, H. Garcia, M. Shalom, A water-splitting carbon nitride photoelectrochemical cell with efficient charge separation and remarkably low onset potential, Angew. Chem. Int. Ed. 57 (48) (2018) 15807–15811.
[52] S. Gao, X. Wang, C. Song, S. Zhou, F. Yang, Y. Kong, Engineering carbon-defects on ultrathin g-C_3N_4 allows one-pot output and dramatically boosts photoredox catalytic activity, Appl. Catal. B Environ. 295 (2021), 120272.
[53] Y. Li, M. Gu, T. Shi, W. Cui, X. Zhang, F. Dong, J. Cheng, J. Fan, K. Lv, Carbon vacancy in C_3N_4 nanotube: electronic structure, photocatalysis mechanism and highly enhanced activity, Appl. Catal. B Environ. 262 (2020), 118281.
[54] W. Wu, J. Zhang, W. Fan, Z. Li, L. Wang, X. Li, Y. Wang, R. Wang, J. Zheng, M. Wu, Remedying defects in carbon nitride to improve both photooxidation and H_2 generation efficiencies, ACS Catal. 6 (5) (2016) 3365–3371.
[55] X. Wu, H. Ma, W. Zhong, J. Fan, H. Yu, Porous crystalline g-C3N4: Bifunctional NaHCO3 template-mediated synthesis and improved photocatalytic H2-evolution rate, Appl. Catal. B Environ. 271 (2020), 118899.
[56] D. Liu, S. Zhang, J. Wang, T. Peng, R. Li, Direct Z-scheme 2D/2D photocatalyst based on ultrathin g-C_3N_4 and WO_3 nanosheets for efficient visible-light-driven H_2 generation, ACS Appl. Mater. Interfaces 11 (31) (2019) 27913–27923.
[57] J. Xu, M. Fujitsuka, S. Kim, Z. Wang, T. Majima, Unprecedented effect of CO_2 calcination atmosphere on photocatalytic H_2 production activity from water using g-C_3N_4 synthesized from triazole polymerization, Appl. Catal. B Environ. 241 (2019) 141–148.
[58] X. Song, Q. Yang, X. Jiang, M. Yin, L. Zhou, Porous graphitic carbon nitride nanosheets prepared under self-producing atmosphere for highly improved photocatalytic activity, Appl. Catal. B Environ. 217 (2017) 322–330.
[59] L. Jiang, J. Li, K. Wang, G. Zhang, Y. Li, X. Wu, Low boiling point solvent mediated strategy to synthesize functionalized monolayer carbon nitride for superior photocatalytic hydrogen evolution, Appl. Catal. B Environ. 260 (2020), 118181.
[60] X. Liang, G. Wang, X. Dong, G. Wang, H. Ma, X. Zhang, Graphitic carbon nitride with carbon vacancies for photocatalytic degradation of bisphenol A, ACS Appl. Nano Mater. 2 (1) (2019) 517–524.
[61] Z. Sun, W. Wang, Q. Chen, Y. Pu, H. He, W. Zhuang, J. He, L. Huang, A hierarchical carbon nitride tube with oxygen doping and carbon defects promotes solar-to-hydrogen conversion, J. Mater. Chem. A 8 (6) (2020) 3160–3167.
[62] E. Picheau, A. Impellizzeri, D. Rybkovskiy, M. Bayle, J.Y. Mevellec, F. Hof, H. Saadaoui, L. Noé, A.C. Torres Dias, J.L. Duvail, Intense Raman D band without disorder in flattened carbon nanotubes, ACS Nano 15 (1) (2021) 596–603.
[63] L.G. Cançado, M.G. Da Silva, E.H.M. Ferreira, F. Hof, K. Kampioti, K. Huang, A. Pénicaud, C.A. Achete, R.B. Capaz, A. Jorio, Disentangling contributions of point and line defects in the Raman spectra of graphene-related materials, 2D Mater. 4 (2) (2017), 025039.